Proceedings of the ASME 2021 International Technical Conference and Exhibition on Packaging and Integration of Electronic and Photonic Microsystems
InterPACK2021
October 26 – 28, 2021, Virtual, Online

InterPACK2021-73269

RACK-LEVEL THERMOSYPHON COOLING AND VAPOR-COMPRESSION DRIVEN HEAT RECOVERY: EVAPORATOR MODEL

Rehan Khalid
Department of Mechanical Engineering
Villanova University
800 Lancaster Avenue
Villanova, PA, USA, 19085
Email: rkhalid@villanova.edu

Raffaele Luca Amalfi
Thermal Management Group
Nokia Bell Laboratories
600-700 Mountain Avenue
Murray Hill, NJ, USA, 07974
Email: raffaele.amalfi@nokia-bell-labs.com

Aaron P. Wemhoff
Department of Mechanical Engineering
Villanova University
800 Lancaster Avenue
Villanova, PA, USA, 19085
Email: aaron.wemhoff@villanova.edu

ABSTRACT

An in-rack cooling system connected to an external vapor recompression loop can be an economical solution to harness waste heat recovery in data centers. Validated subsystem-level models of the thermosyphon cooling and recompression loops (evaporator, heat exchangers, compressor, etc.) are needed to predict overall system performance and to perform design optimization based on the operating conditions. This paper specifically focuses on the model of the evaporator, which is a finned-tube heat exchanger incorporated in a thermosyphon cooling loop. The fin-pack is divided into individual segments to analyze the refrigerant and air side heat transfer characteristics. Refrigerant flow in the tubes is modeled as 1-D flow scheme with transport equations solved on a staggered grid. The air side is modeled using differential equations to represent the air temperature and humidity ratio and to predict if moisture removal will occur, in which case the airside heat transfer coefficient is suitably reduced. The louver fins are modeled as individual hexagons and are treated in conjunction with the tube walls. A segment-by-segment approach is utilized for each tube and the heat exchanger geometry is subsequently evaluated from one end to the other, with air property changes considered for each subsequent row of tubes. Model predictions of stream outlet temperature and pressure, refrigerant outlet vapor quality and heat exchanger duty show good agreement when compared against a commercial software.

Keywords: *Analytical modeling, Data centers, Electronics cooling, Liquid-cooling, Mathematical modeling, Modeling*

NOMENCLATURE

Roman	
A	cross-sectional area, m^2
$c_{p,a}$	specific heat of air, $\mathrm{J/(kg.K)}$
D_r	root diameter of the fin, m
D_t	tip diameter of the fin, m
finPitch	number of fins per inch of tube length, m^{-1}
G	mass flux, $\mathrm{kg/(m^2.s)}$
g	gravitational constant ($9.80685\ m^2/s$)
h	mass-based enthalpy, J/kg
$\bar{h}$	average flow-weighted enthalpy (at position z), J/kg
$\bar{h}_\rho$	average density-weighted enthalpy (at position z), J/kg
Le	Lewis number
L_{finned}	finned length of the heat exchanger tube, m
$N_{fins,tot}$	total number of fins on heat exchanger
p	pressure, Pa
P	wetted perimeter , m
P_d	diagonal pitch, m
P_l	longitudinal pitch (in line of flow), m
P_t	tube or transverse pitch (perpendicular to line of flow), m
$\bar{q}''$	average heat flux, $\mathrm{W/m^2}$
s	fin spacing, m
L	fin height, m
L_t	total length of tube, m
n_t	number of tubes in a row
n_r	number of rows
N	total number of tubes ($n_r * n_t$)
Ref.	refrigerant
u	velocity, m/s
w	fin thickness, m

x	flow quality
$\hat{x}$	static quality (mass-based)
x	axis perpendicular to direction of air flow
y	axis parallel to direction of air flow
z	axis in line with refrigerant flow

Greek Letters

α	heat transfer coefficient, $\mathrm{W/(m^2.K)}$
α_m	mass transfer coefficient
Δ	increment
γ	void fraction
η	efficiency
$\dot{m}$	mass flow rate, $\mathrm{kg/s}$
ρ	density, $\mathrm{kg/m^3}$
$\bar{\rho}$	average density (at position z), $\mathrm{kg/m^3}$
$\bar{\rho}_m$	average momentum density (at position z), $\mathrm{kg/m^3}$
$\bar{\tau}$	average shear stress, Pa
θ	angle of inclination (to horizontal), °
ω	humidity ratio (moist air), $\mathrm{kg\ (vapor)/kg\ (dry-air)}$

Subscripts

1ϕ	Single-Phase
a	Air
f	Saturated Liquid
g	Saturated Vapor
G	Generation
h	Heated
i	Coordinate used to denote Staggered Grid
I	Coordinate used to denote Main/Scalar Grid
m	Mean / Mass
mfld	Manifold
o	Overall
r	Refrigerant
sat	Saturated
tot	Total
w	Wall

Acronyms

CAPEX	Capital Expenditure
COP	Coefficient of Performance
CRAH	Computer Room Air Handler
DC	Data Center
EDR	Exchanger Design & Rating
EEV	Electronic Expansion Valve
HTC	Heat Transfer Coefficient
HX	Heat Exchanger
ITE	Information Technology Equipment
LV	Liquid-Vapor
OEM	Original Equipment Manufacturer
OPEX	Operating Expenditure
RDHX	Rear Door Heat Exchanger
WHR	Waste Heat Recovery

1. INTRODUCTION

Datacenters have been traditionally cooled by supplying cold air through an underfloor plenum [1], [2] with ASHRAE recommended IT inlet air temperatures in the range of 18-27°C [3]. The exhaust air temperatures are, in turn, below 50°C, as recommended by major OEMs. This scheme presents disadvantages in terms of the electric energy consumed by the cooling system and the discharge of heat to the ambient without any intermediate use. The waste heat is typically high in quantity but low in quality. In turn, there remains the potential to:

- Reduce the cooling power requirement of legacy DCs
- Capture, transport and reuse this heat for various purposes

Further, an increasing datacenter average rack power density over the past three years [4] represents a growing opportunity to switch to liquid cooling. Liquid cooling allows thermal engineers to operate with condensing temperatures in the 40-60°C range, depending on the choice of a single or multiphase liquid cooling system [5], [6] while maintaining chip case temperatures within reliability limits. The use of vapor-compression driven liquid cooling allows for condensing temperatures up to 90°C [7]. A higher condensing temperature leads to three major benefits such as:

- Effective waste heat harvesting
- Monetary benefits gained by a reduction in cooling system energy costs and further capital gain via WHR
- Reduced carbon footprint via lesser CO_2 emissions (and possible financial gain if a local carbon tax is in place)

To that end, this study presents a mathematical model of an evaporator incorporated in a novel thermal management solution that not only efficiently cools and captures heat from hardware components in datacenters and telecom central offices, but also allows for heat recovery via a traditional heat pump. Figure 1 shows a schematic of the system under study.

The equipment to be cooled (computer servers in this case) are contained in an air-cooled rack. The ITE is cooled by air that is continuously circulated within the cabinet, while the air itself is cooled via an air-to-refrigerant heat exchanger that is the evaporator of a thermosyphon loop. In particular, the evaporator is a finned tube heat exchanger that is widely used in refrigeration and air-conditioning applications. The refrigerant flows in a thermosyphon loop between a source and sink (evaporator and condenser, respectively). A reservoir tank (LV-separator) connects the two HXs, which physically separates the refrigerant liquid and vapor phases.

The vapor refrigerant either can reject heat directly through a water-cooled condenser or be driven through a heat pump, thereby boosting its pressure (and temperature) for enhanced heat recovery. The high temperature condenser cooling water can then be used for various applications such as district heating, as service fluid within process industries, or as potable water in the same or co-located buildings. Alternatively, the condenser of Figure 1 can be replaced or augmented with an absorption chiller to produce cold water, which can be supplied to an HVAC system or used as potable water in the summer months. The hot and/or

cold water thus produced can be a source of revenue for the datacenter owner. If priced correctly, the incoming revenue can more than offset the cost of running the compressor, thereby generating a yearlong profit for the datacenter owner. The reader is referred to [8] for case studies detailing the applications and efficacy of the heat recovery system.

From a thermodynamic perspective, the amount of heat recovered by the cooling water in the condenser of Figure 1 will be greater than the electric power needed to run the compressor, since heat pumps have a COP greater than unity [9]. From an operating standpoint, achieving a COP of three (3) for the proposed heat pump system would put it at par with commercially available air-conditioners, which are ubiquitous, thermodynamically efficient and cost-effective, thereby proving its practicality. As an example, the UK government incentivizes heat pumps with a COP greater than or equal to 2.7 for use in district heating applications [10]. Further, a traditional heat pump can boost the temperature of its working fluid up to 90°C [7], custom-built high temperature and very high temperature heat pumps can boost it up to 120°C and 140°C respectively [11], [12], [13] while industrial heat pumps can boost it up to 150°C [14]. Such high condensing temperatures can subsequently be used to generate hot water at around 70°C, which is ideally suited for revenue generating applications like district heating [10], bottling and meat packaging, since the elevated temperature kills bacteria contained in the water.

This close-coupled cooling technique resembles near-coupled cooling techniques such as passive rear-door heat exchangers (RDHXs), where the air from the data center (DC) whitespace enters the rack, cooling the ITE and then exchanging heat with chilled water flowing through a finned-tube HX mounted at the rear of the rack [15], [16]. No cabinet fans are involved [16], saving on their power consumption. In contrast, active RDHXs employ cabinet fans for a more uniform airflow across the cabinet [17]. Similarly, refrigerant-based RDHXs rely on low-pressure refrigerant as opposed to water to cool the air from the ITE exhaust [18]. Modular cooling is another category of DC cooling technology that relies on modular solutions e.g. overhead and in-row coolers to cool the ITE.

The main disadvantages of these near-coupled techniques is that they i) require a CRAH unit to move the air around the DC whitespace and through the racks housing the ITE equipment ii) require use of a chiller and/or cooling tower to supply chilled water or refrigerant to the RDHXs. Moreover, modular cooling techniques require the use of pumps to move the liquid refrigerant or chilled water, thereby decreasing reliability of the cooling solution in case of leaks and increases its CAPEX and OPEX.

The proposed solution is a close-coupled technique where the air never leaves the rack (enclosed cabinet). It offers the following advantages compared to RDHXs and modular cooling technologies:

i. Eliminates the CAPEX and OPEX associated with costly CRAH units.
ii. Relies on self-regulating, passive thermosyphon-based cooling, thus eliminating moving parts such as pumps and gears, thereby reducing maintenance cost, increasing reliability of the cooling system and reducing ITE downtime
iii. Vapor from the LV-separator can be directly fed to a central rooftop condenser, which can be air-cooled to eliminate the expenditure of a chiller or cooling tower
iv. Alternately, the vapor can be sent through a compressor (heat pump) before going through a water-cooled condenser or absorption chiller. The hot or cold water created can then be used for economic activity generation [8], as explained above

Finned-tube heat exchangers have been widely studied over the past 50 years. Greater interest was initially placed in studying the airside due to its higher thermal resistance, thereby influencing the overall system performance. Eminent among these early studies are the works of McQuiston [19]-[20] and Rich [21] in quantifying the air-side performance of these HXs, in particular the heat transfer coefficient using Colburn j-factors and the pressure drop, evaluated separately for the tubes and fins. The work of Schmidt [22] and subsequently Webb [23] in modeling the continuous fin geometry as discrete hexagons and further approximating the geometry as circular/annular fins is of paramount importance. This allowed the determination of the fin efficiency with ease using trigonometric functions as opposed to more complex Bessel functions. Flow boiling of refrigerants continues to be actively explored till date, with the works of Kandlikar [24]-[25], Shah [26] and Kays & London [27] standing out for their contribution to Nusselt number correlation development and for their comprehensive work on characterizing the performance of compact heat exchangers.

The current study is based on the work of Qiao et. al [28] to model and predict the performance of a finned-tube HX. The heat exchanger functions as an evaporator, designed to operate as part of a thermosyphon for a novel thermal management solution. The model incorporates three new features not present in the earlier model, which are used to predict the performance of the evaporator for a given set of inlet stream conditions. Furthermore, the model is used to analyze the effect of sub-cooling on the evaporator performance and outlet stream conditions, critical to the intended thermal management application. It has to be mentioned that an accurate model of the evaporator is extremely important for predicting the thermal performance of the system it is placed in and for benchmarking purposes.

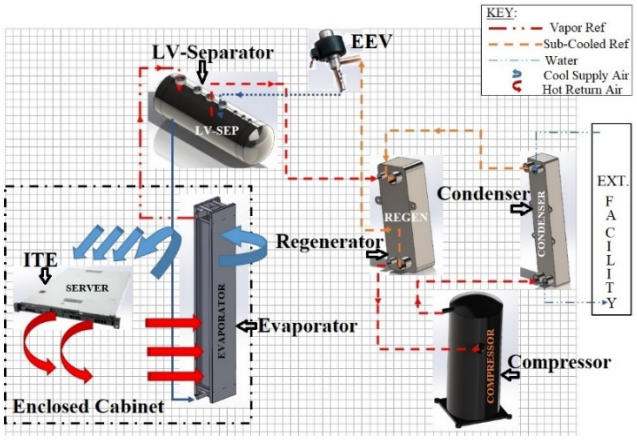

FIGURE 1: PROPOSED THERMAL MANAGEMENT AND HEAT RECOVERY SYSTEM.

2. EVAPORATOR GEOMETRY

The evaporator is a finned-tube heat exchanger incorporated in a thermosyphon loop. The evaporator geometry as fabricated divides the HX into two identical finned tube sections, with three rows of tubes in each section, where each row is seven tubes wide. Thus, each section consists of 21 vertical, single-pass tubes with the entire evaporator containing 42 tubes. A CAD model of the overall finned-tube HX (evaporator) is shown in Figure 2, while Figure 3 shows a close-up of the inlet manifold and tubing.

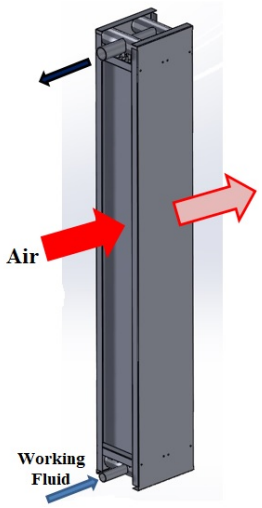

FIGURE 2: EVAPORATOR GEOMETRY.

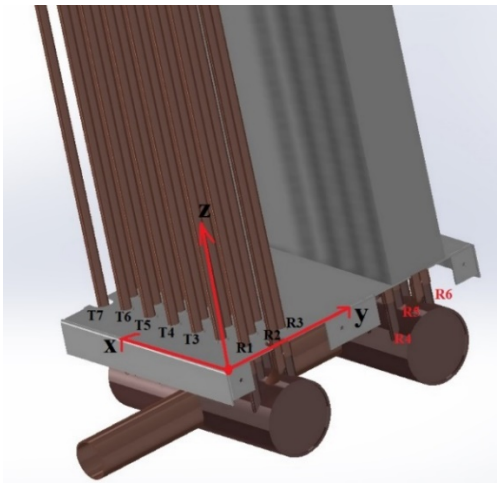

FIGURE 3: EVAPORATOR INLET MANIFOLD WITH THE ROWS AND TUBES IN EACH ROW LABELED.

3. MODELING STRATEGY

The evaporator geometry is modeled using the following assumptions for the air and refrigerant sides:

Refrigerant Side

- No flow maldistribution between tube bundles, tube rows and individual tubes;
- Incoming flow splits equally among all tubes;
- Modeling takes place in the y-z plane;
- Only one tube modeled from each row;
- Each tube in a given row faces the same conditions inside and outside;
- Viscous heating is neglected through the inlet and outlet headers. Thus, the refrigerant temperature and enthalpy entering the tubes are the same as that entering the HX.

Air Side

- Incoming air mass flow rate splits equally among all tubes in a given row;
- No mixing on the air-side takes place in the z-direction due to fins;
- Mixing in the y-direction due to back flow does not impact results - same stream packet impacts the next ref cell;
- No significant temperature gradients exist in the x-direction;
- The output from one row of tubes becomes the input for the next row of tubes.

The above assumptions simplify the geometry from 3-D to 2-D. The resulting geometry can then be depicted as shown in Figure 4 below. The simplified geometry is used for further analysis of the evaporator. It is advantageous to use this geometry since it makes the resulting computation easier and faster while still preserving the flow physics, and therefore the model predictive capabilities, as shown later in this study.

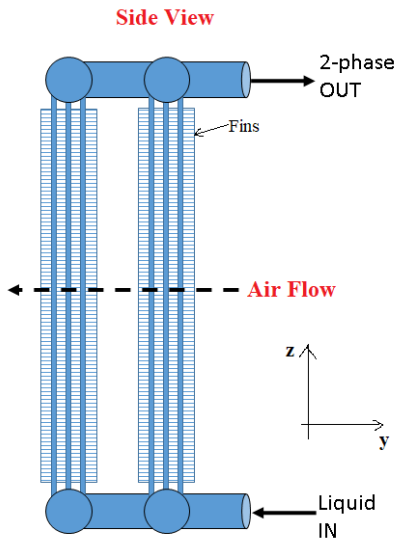

FIGURE 4: SIMPLIFIED EVAPORATOR GEOMETRY FOR ANALYSIS.

A segment-by-segment approach is utilized to solve the simplified 2-D geometry. A grid can then be overlaid on the geometry of Figure 3, as shown in Figure 5. Each hatched square is a segment and forms the basic unit on which the transport equations for the air and refrigerant side are evaluated.

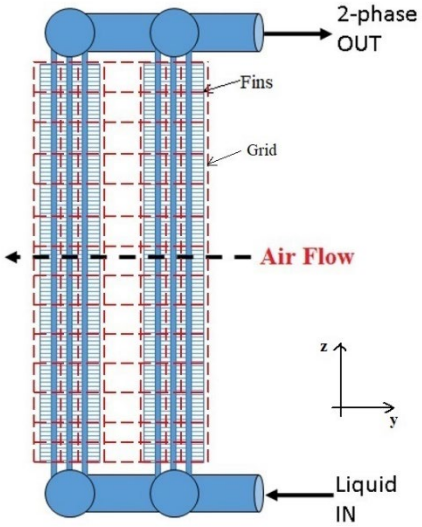

FIGURE 5: GRID USED FOR ANALYZING THE 2-D EVAPORATOR GEOMETRY.

4. MODEL DEVELOPMENT

4.1. Air Side

The air side is modeled via mass and energy balances in the y-direction for each grid segment, as shown in Figure 6 below.

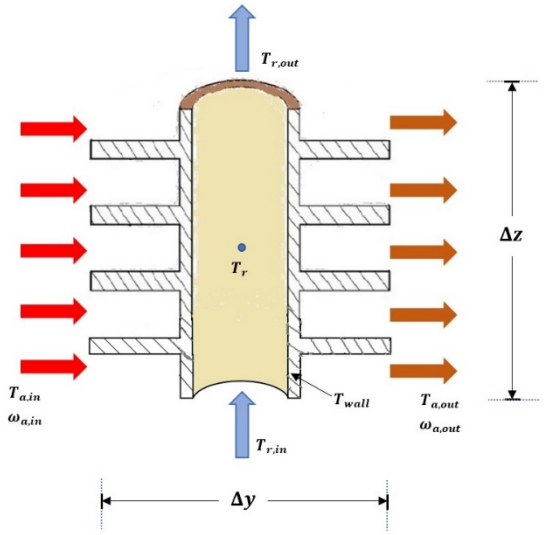

FIGURE 6: DETAILED VIEW OF A SINGLE SEGMENT, USED FOR AIRSIDE ANALYSIS.

This approach results in the following ODEs:

Energy Balance:

$$\dot{m}_a c_{p,a} \frac{dT_a}{dy} \Delta y = \alpha_a \left(A_{o,tube} + \eta_{fin} A_{o,fin}\right)(T_{wall} - T_a) \quad (1)$$

Mass Balance:

$$\dot{m}_a \frac{d\omega_a}{dy} \Delta y = \alpha_m \left(A_{o,tube} + \eta_{fin} A_{o,fin}\right) \cdot \min(0, \omega_{w,sat} - \omega_a) \quad (2)$$

where

$$\alpha_m = \frac{\alpha_a}{c_{p,a} Le^{2/3}} \quad (3)$$

is the mass transfer coefficient and Le is the Lewis number, used to incorporate the Lewis analogy for simultaneous heat and mass transfer, and $Le^{2/3} \sim 0.90$, according to Keuhn et. al [29]. Finally, $\omega_{w,sat}$ is the humidity ratio of saturated air, evaluated at T_{wall}.

Analytically solving the above equations for each grid segment gives the following equations for the air outlet temperature and humidity ratio:

$$T_{a,out} = T_{a,in} + \left(T_{wall} - T_{a,in}\right)\left[1 - e^{-\left(\frac{M}{\dot{m}_a c_{p,a}}\right)}\right] \quad (4)$$

$$\omega_{a,out} = \omega_{a,in} + \left[1 - e^{-\left(\frac{M}{\dot{m}_a c_{p,a} Le^{2/3}}\right)}\right] \cdot \min(0, \omega_{w,sat} - \omega_a) \quad (5)$$

where the terms used to define the total air-side heat transfer area is grouped into the constant M, defined as follows:

$$M \equiv \alpha_a \left(A_{o,tube} + \eta_{fin} A_{o,fin}\right) \quad (6)$$

The term $A_{o,tube}$ represents the overall exposed base surface area, sometimes also referred to as the prime area. This is the area on the tube wall that is not occupied by the fins. Moreover, $A_{o,fin}$ represents the overall finned surface area. These can be easily determined based on the geometry of the finned tube HX, as identified in Figure 6. The efficiency of a single fin, η_{fin}, can be determined based on the expressions identified in the Section on Tube Wall and Fins.

The air-side heat transfer coefficient, α_a, is determined using the Colburn j-factor approach based on the correlation developed by McQuiston and Parker [30]. Since a segment-by-segment approach is utilized to analyze the heat exchanger geometry, the heat transfer coefficient is determined individually for each segment, based on the air properties entering a given row.

The air side pressure drop cannot be computed directly using Eqs. (1) and (2). While it is not important to consider the pressure drop in most air-cooled HXs for refrigeration applications, it is vital to determine the air-side pressure drop in this case due to two reasons:

i. It allows for calculation of the airside properties using CoolProp's humid air library, which requires three state inputs (T, P & ω are used here);
ii. To ensure that the pressure drop across the evaporator (and IT equipment) can be offset by the static pressure rise due the cabinet fans.

Hence, the air-side pressure drop is computed separately and is the sum of the pressure drop over the bare tubes and the fins. The work of Rich [21] is used to determine the pressure drop due to the fins, while the pressure drop across the bare tube bank is determined based on the work of Zukauskus & Ulinskas [31]. The pressure drop, like the heat transfer coefficient, is computed individually for each tube row.

4.2. Tube Wall and Fins

The two fluids (air and refrigerant) interact through the tube wall, therefore the wall temperature links the air and refrigerant sides. The following assumptions are used to model the tube wall and fins:

- Tube wall is assumed to be thin;
- Fin temperature profile is steady-state and represented by the fin efficiency;
- Tube wall and fin temperatures are lumped into a single temperature.

Based on the above assumptions, the fin base temperature is equal to the tube wall temperature, which can then be used to represent the combined fin and tube wall thermally. Per assumption of a thin wall, a surface energy balance on the tube wall yields:

$$\dot{E}_{in} - \dot{E}_{out} = 0 \tag{7}$$

$$\dot{q}_a - \dot{q}_r = 0 \tag{8}$$

$$\dot{m}_a\left[c_{p,a}\left(T_{a,in} - T_{a,out}\right) + \left(\omega_{a,in} - \omega_{a,out}\right)\Delta h_{fg}\right] - \alpha_r A(T_w - T_r) = 0 \tag{9}$$

Substituting equations (4) and (5) for $T_{a,out}$ and $\omega_{a,out}$ respectively and re-arranging yields the following equation for the tube wall temperature, where A is based on the tube outer diameter of the heated perimeter:

$$T_{wall} = \frac{\alpha_r A T_r + \dot{m}_a c_{p,a}\left(1-e^{-(M/\dot{m}_a c_{p,a})}\right)T_{a,in} + Y}{\dot{m}_a c_{p,a}\left(1-e^{-(M/\dot{m}_a c_{p,a})}\right) + \alpha_r A} \tag{10}$$

where M is defined by Eq. (6) and Y is given by

$$Y = [e^{-M/(\dot{m}_a c_{p,a} Le^{2/3})} - 1] * \min\left(0, \omega_{w,sat} - \omega_{a,in}\right) * \Delta h_{fg} \tag{11}$$

To determine the fin efficiency, fins are approximated as hexagonal and further represented as annular fins (Schmidt [22]). This concept is illustrated in Figures 7 and 8, respectively. The efficiency of a single annular fin is readily determined using either of the following techniques: (i) from tabulated correlations based on the modified Bessel functions (e.g. Eq. 3.91 in [32]); (ii) from the Webb equation [23].

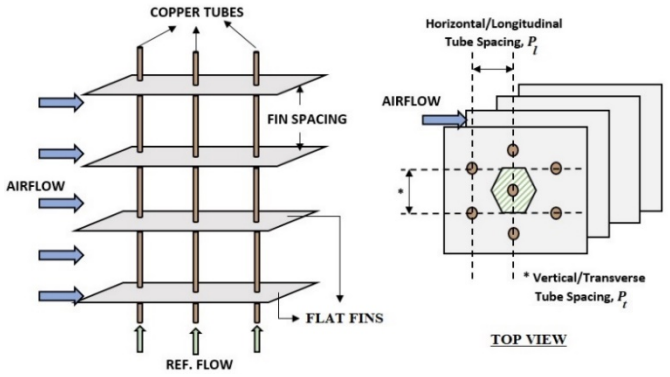

FIGURE 7: FIN DEPICTION - CONTINUOUS FLAT FINS APPROXIMATED AS DISCRETE HEXAGONS.

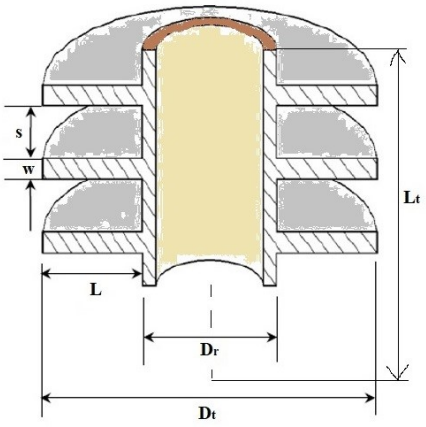

FIGURE 8: FIN DEPICTION - HEXAGONAL FINS FURTHER APPROXIMATED AS CIRCULAR/ANNULAR.

4.3. Refrigerant Side

The refrigerant side is evaluated based on the steady-state form of the three transport equations [33]:

$$\frac{d}{dz}(GA) = 0 \tag{12}$$

$$\frac{d}{dz}\left(\frac{G^2A}{\bar{\rho}_m}\right) = -A\frac{dp}{dz} - \bar{\tau}_w P - \bar{\rho} g A sin\theta \tag{13}$$

$$\frac{d}{dz}\left(G\bar{h}A\right) = P_h\bar{q}'' + A\bar{q}_G - gGAsin\theta \tag{14}$$

where G represents the mass flux of the refrigerant flowing through the heat exchanger tubing, A is the cross-sectional area based on the tube inner diameter of the wetted perimeter, while the two-phase densities and enthalpies are calculated as defined in [33].

For single-phase flow, the density can be approximated as constant throughout the tube's cross-section. Hence, all the densities and enthalpies collapse down to one value each:

$$\bar{\rho}_m = \bar{\rho} = \rho_{1\phi} \tag{15}$$

$$\bar{h}_\rho = \bar{h} = h_{1\phi} \tag{16}$$

For two-phase flow, the densities and enthalpies are calculated as:

$$\bar{\rho} = \rho_g\gamma + \rho_f(1-\gamma) \tag{17}$$

$$\frac{1}{\bar{\rho}_m} = \frac{1}{\rho_g}\frac{x^2}{\gamma} + \frac{1}{\rho_f}\frac{(1-x^2)}{(1-\gamma)} \tag{18}$$

$$\bar{h}_\rho = h_g\hat{x} + h_f(1-\hat{x}) \tag{19}$$

$$\bar{h} = h_g x + h_f(1-x) \tag{20}$$

where γ is the void fraction (gas volume fraction), x is the flow quality (gas weight-rate fraction) and $\hat{x}$ is the static quality (gas mass-fraction), as defined in [33].

A slip-ratio correlated model for the void fraction is utilized for purposes of this study since it is easy to implement, causes no significant numerical complications and is more accurate than homogenous flow model for low mass flux two-phase flows ($\leq 2700\ kg/(m^2.s)$) [34]. Based on this model, the flow quality can be correlated to the void fraction using the following standard expression [35]:

$$x = \frac{\gamma^{1\backslash q}}{\gamma^{1/q} + \left[\frac{1}{c}\left(\frac{\rho_f}{\rho_g}\right)^r\left[\frac{\mu_g}{\mu_f}\right]^s\right]^{1\backslash q}(1-\gamma)^{1\backslash q}} \tag{21}$$

The constants and exponents used to determine the flow quality, x, are based on the Smith model [36], while the constants and exponents for the homogenous model are used to determine the static quality, $\hat{x}$. Both sets of constants and exponents are tabulated in Table 1 below:

Table 1: CONSTANTS AND EXPONENTS FOR TWO-PHASE VOID FRACTION MODELS.

Model	c	q	r	s
Homogenous	1	1	1	0
Smith	0.79	0.78	0.58	0

The above equations are discretized on a back-staggered grid, as shown in Fig. 9, to decouple velocity from pressure. Thus, the momentum and energy equations are solved on the main/scalar Control Volume (CV) with the variables evaluated at the centroid of the cells (nodes denoted by $'I'$). The momentum equation, however, is solved on the staggered CV, with the velocities/mass flow rates determined at the intersection or faces of the main CV (nodes denoted by $'i'$).

The final form of the discretized equations are presented below, where the energy generation term is dropped from Eq. (14), since no heat source or sink is present in the entire HX, and by extension, within the tubes:

$$\dot{m}_{i+1} = \dot{m}_i \tag{22}$$

$$A[p_{I-1} - p_I] = \frac{\dot{m}_i^2}{A}\left[\frac{1}{\bar{\rho}_{m\,I+1} + \bar{\rho}_{m\,I}} - \frac{1}{\bar{\rho}_{m\,I-1} + \bar{\rho}_{m\,I-2}}\right] + \bar{\tau}_{w_i} P\Delta z + \left(\frac{\bar{\rho}_I + \bar{\rho}_{I-1}}{2}\right) gAsin\theta\Delta z \tag{23}$$

$$\dot{m}_i\left[\bar{h}_I - \bar{h}_{I-1}\right] = P_h\bar{q}_I''\Delta z - \left(\frac{\dot{m}_{i+1} + \dot{m}_i}{2}\right) gsin\theta\Delta z \tag{24}$$

Eq. (22) results from recognizing that $GA = \dot{m}$ is the mass flow rate of the refrigerant flowing through a given tube and is constant throughout. Eq. (23) in the presented form allows one to determine the pressure at a given node by knowing the pressure at the previous node and the appropriate components of the pressure drop between the two nodes; this pressure gradient sustains the flow through the vertical HX tubes. The first term on the RHS of Eq. (23) is obtained by using a second-order differencing scheme and represents the momentum pressure drop between nodes $'I'$ and $'I-1'$. The second and third term represent the frictional and static pressure drop components, respectively. Finally, Eq. (24), as presented, allows one to determine the average flow-weighted enthalpy of the refrigerant at a given node by knowing the same value at the previous node and the cell heat flux. The upwind differencing scheme is utilized to discretize the convective flux terms on the LHS of Eq. (24). Note that the heated perimeter, P_h, differs from the wetted perimeter, P, where the former is evaluated based on the tube outside diameter, or root diameter, d_r, and the latter is evaluated using the tube inner diameter.

Eq. (22) through (24) are solved explicitly with the mass flow rate, pressure and average flow-weighted enthalpy entering a tube as boundary conditions. The number of grid cells are

strategically chosen so that an integer number of fins occupy each cell and the same number of fins are present in each cell to preserve grid symmetry. Thus, the number of grid cells comprise an array, where each value is a factor of the total number of fins present in the HX, which is determined as the product of fin pitch and tube finned length.

Appropriate correlations from the literature are used to compute the refrigerant side HTC. The correlation of Kays and London [27] is used to determine the single-phase HTC while the generalized Kandlikar correlation [25] for flow boiling inside vertical and horizontal tubes is used for two-phase flow. The primary intended working fluid for this cooling and heat recovery system is R-245fa. Note that the fluid dependent parameter, F_{fl}, in Kandlikar's correlation is not given for this fluid, so a value of 1.304 is used that corresponds to that of R-11 since R-245fa is its direct replacement.

Finally, the discretized set of equations (22) – (24) is solved explicitly. However, the momentum term on the RHS of Eq. (23) involves $\bar{\rho}_{m\,I+1}$, which requires knowing the state of the cell next to the current one. Since that is unknown, the momentum pressure term is dropped from the discretized equation; instead, the momentum pressure drop is artificially introduced. The pressure drop due to momentum change is neglected for single-phase flow since density changes are negligible, and it is computed using the expression given by Hiller & Glicksman [37], which can be integrated over the cell length, with limits on the previous and current node static quality.

Similarly, the friction pressure drop is computed using the Moody (Darcy) friction factor instead of computing the wall shear stress, which is not straightforward to determine. For single-phase flow, the friction factor is determined using the standard form of the pipe equation, with $f = 64/Re$ for laminar flow assuming a smooth pipe and by solving the Colebrook-White equation for a rough pipe. For two-phase flow, the friction pressure drop is computed using the correlation proposed by Muller-Steinhagen and Heck, which is an empirical correlation based on a large data set, is easy to use, and as per the authors, gives good predictions compared to other, more complicated correlations [38].

In short, the calculation procedure for the refrigerant side proceeds as follows:

1. Define p and $\bar{h}$ as state variables
2. $\dot{m}$, $\bar{\rho}$, $\bar{\rho}_m$ are algebraic variables; also $\bar{h}_\rho$
3. Choose appropriate number of grid cells
4. Assign $\dot{m}_{in}$, p_{in} & $\bar{h}_{in}$ as BCs; $\bar{h}_{in}$ for 1ϕ only
5. If single-phase
   i. Get ρ from property routines
   ii. Get $\bar{\rho}_m$ and $\bar{h}_\rho$ using Eqs. (15)-(16)

   Else
   i. Get $\bar{\rho}_l$ from property routines, including ρ_f & ρ_g
   ii. Solve for γ using definition of $\bar{\rho}$
   iii. Find x using Eq. (21) and appropriate model e.g., Smith
   iv. Find $\hat{x}$ using Eq. (21) and homogenous model
   v. Get $\bar{\rho}_m$ and $\bar{h}_\rho$ using Eqs. (17)-(18)
6. Get HTC using appropriate correlations
7. Get dP_{mom} & dP_{fric} using suitable expressions; dP_{static} using eqn. (23)
8. Solve Eqs. (22) – (24) to obtain p_I & $\bar{h}_I$
9. Repeat steps 5 – 8 for $I = 2 \rightarrow N$

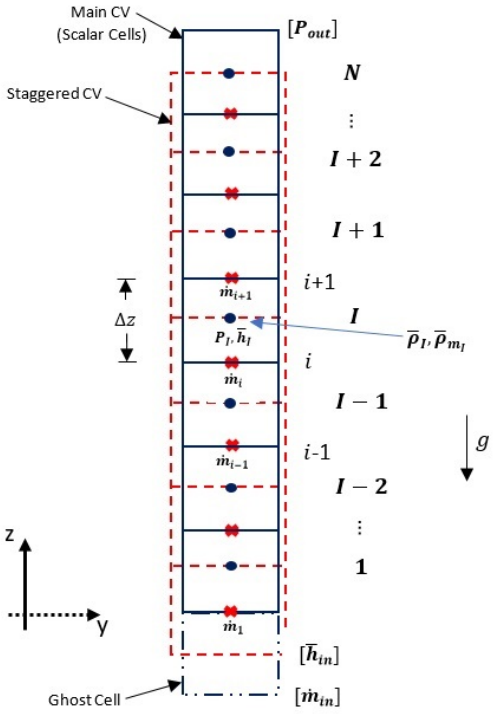

FIGURE 9: GRID USED TO DISCRETIZE THE REFRIGERANT SIDE.

The refrigerant pressure drop through the inlet and outlet manifold is determined based on the header geometry. Both headers are symmetrical and have the same dimensions, with the exception of the inlet and outlet tube diameter. The pressure drop through the inlet and outlet tube is determined in the same manner as the refrigerant pressure drop through the vertical HX tubes, except that an inclination angle of zero degrees is used (versus 90° for the former). The refrigerant experiences expansion and contraction as it flows from the main header tube into the header manifold and subsequently into the vertical HX tubes. These result in a pressure rise and drop, respectively, and are calculated using the K-factors provided in [39]. Finally, based on the header's symmetrical design (Fig. 3), the pressure drop for the first half of the header (inlet to first three rows of tubes) is calculated separately and then used to further determine the pressure drop for the second half of the header (next three rows of tubes).

Lastly, the enthalpy and pressure exiting the two tube bundles are averaged to yield the refrigerant outlet stream conditions, after accounting for the pressure drop through the outlet header. Similarly, the enthalpy and humidity ratio are averaged on the air side to yield the air-stream outlet conditions.

The flowchart of Fig. 10 outlines the steps needed to solve the evaporator geometry for a given set of inlet stream conditions.

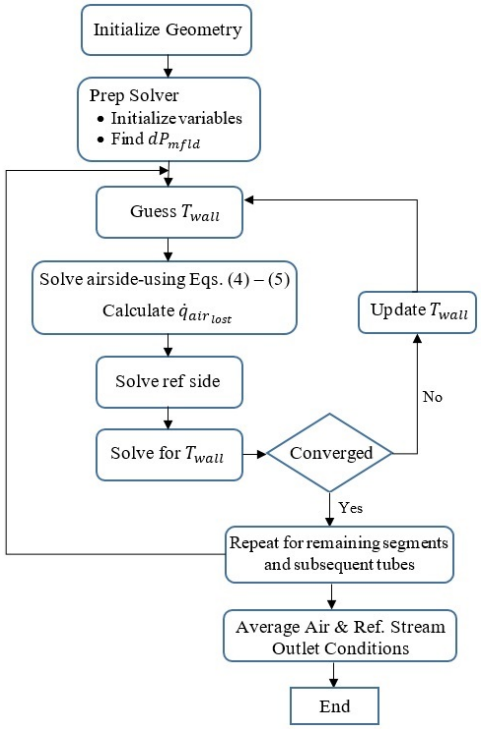

FIGURE 10: EVAPORATOR SOLVER FLOWCHART.

5. MODEL VALIDATION

Prior to validating the model, a grid resolution study is performed. This is essential in balancing model accuracy with computational cost. To ensure that the HX duty is independent of the grid size, the number of cells is chosen to go beyond the maximum number of cells initially specified (i.e., grid sizes that feature half and quarter number of fins per cell is also included for this purpose). The resulting HX duty trend is shown in Fig. 11. In particular, 2254 grid segments are selected for further model validation based on the trend identified in the figure.

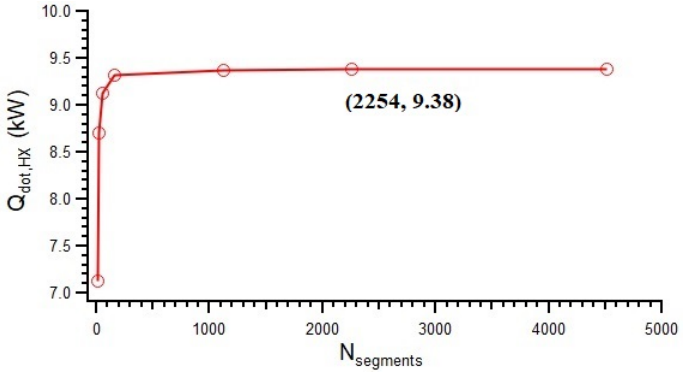

FIGURE 11: EVAPORATOR MODEL GRID INDEPENDENCE STUDY.

The model is validated against existing validated commercial software, Aspen EDR [40], [41] for a single set of inlet conditions. The geometry of the finned-tube HX under study is specified for an air-cooled HX type object in Aspen EDR, along with the inlet stream conditions specified in Table 2. These conditions are chosen to best mimic the conditions that would be prevalent within the rack and would maximize overall system performance, based on earlier system-level simulations carried out in Aspen Plus. In particular, the evaporator air inlet temperature of 50°C is the maximum ITE exhaust temperature permitted by OEMs. In addition, the maximum air mass flow rate permitted by the cabinet fans is 3600 kg/h [42].

TABLE 2: EVAPORATOR INLET STREAM CONDITIONS.

Parameter	Air	Refrigerant
T_{in} (°C)	50	20
P_{in} (bar)	2	2
$\dot{m}$ (kg/s)	3600	1800

The resulting outlet stream conditions along with the exchanger duty and simulation time are compared in Table 3. As can be seen, the outlet stream conditions for both the refrigerant and airside exhibit a near perfect match, while the discrepancy in refrigerant side outlet quality can be attributed to the choice of the single-phase heat transfer correlation, which affects the length of the single-phase and subsequently two-phase region. A lower outlet quality denotes a smaller length for the two-phase region for the given model versus that predicted by Aspen EDR. Effectively, however, the comparison confirms that the outlet refrigerant static quality is very low (liquid dominated). The resulting exchanger duty is within 15% of that reported by Aspen.

TABLE 3: EVAPORATOR OUTLET CONDITIONS.

Stream Parameter	Air		Refrigerant	
	Model	EDR	Model	EDR
T_{out} (°C)	41.2	41.8	30.8	30.8
P_{out} (bar)	1.999	1.999	1.83	1.81

Overall Parameter	Model	EDR
ΔP_{air} (Pa)	135	119
$x_{out,ref}$	0.02	0.10
$\dot{Q}_{HX}$ (kW)	9.17	8.20
Sim. Time (s)	322	12

6. PARAMETRIC STUDY

The degree of sub-cooling is a critical parameter that influences the performance of an evaporator or condenser, particularly in a vapor-compression cycle. Hence, the effect of sub-cooling on the heat exchanger duty, air side outlet temperature and refrigerant outlet mass-based quality is analyzed in this section, compared to the reference case with almost no sub-cooling. The reference case corresponds to an evaporator inlet temperature corresponding to the saturation temperature of 2 bar for R-245fa, plus an additional 0.10 °C to offset numerical instabilities resulting from the evaporator inlet temperature being within $1 * 10^{-4}$ of the saturation temperature. All transport properties are evaluated using CoolProp [43], [44]. Results are shown in the three plots of Figure 12.

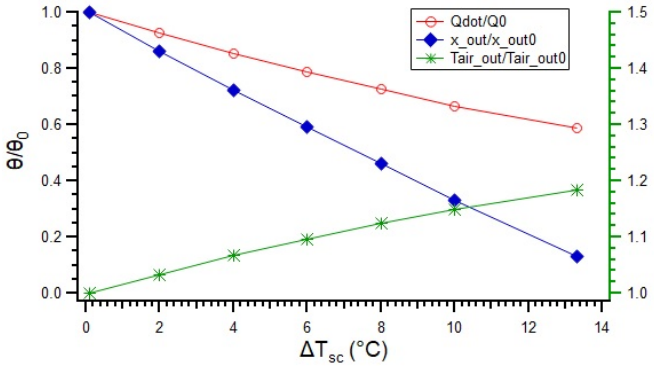

FIGURE 12: EFFECT OF SUB-COOLING ON HEAT EXCHANGER PARAMETERS.

Figure 12 shows that the heat exchange capability of the evaporator goes down by about 40% as the inlet sub-cooling increases from nearly zero to about 13.3°C. The primary reason for this behavior is that the refrigerant now stays in single-phase longer (more sensible heat transfer), thereby decreasing the advantage of the higher HTCs afforded by phase change due to the presence of latent heat. This trend can be clearly observed from the blue curve of Fig. 12, which shows that the ratio of the refrigerant outlet quality nearly goes to zero, implying that the actual refrigerant quality nearly goes to zero for the higher sub-cooling. The smaller amount of heat transfer to the refrigerant, thus, leads to a lesser heat loss from the airside, which translates into higher air temperatures exiting the evaporator and going into the ITE.

Finally, for a target cabinet heat load of 10 kW and a maximum ITE exhaust temperature of 50°C leads to an ITE inlet temperature of 40°C, which can be achieved for a sub-cooling of approximately 10°C for the given refrigerant inlet pressure and mass flowrate.

7. SUMMARY & CONCLUSIONS

A model for a finned-tube heat exchanger is presented in this study, based on the work of Qiao et. al [28]. The heat exchanger acts as an evaporator and is part of a novel thermal management solution proposed to cool hardware components in data centers and telecom central offices.

The model uses the geometry of the heat exchanger to predict the refrigerant pressure drop in the inlet and outlet headers of the exchanger, primarily due to wall friction and sudden expansion and contraction of the refrigerant. The model further artificially incorporates the momentum pressure drop on the refrigerant side, by integrating the expression proposed by Hiller & Glicksman [37] with suitable limits, as opposed to using the discretized momentum equation. Finally, the model incorporates the pressure drop on the air side, as a mean to judge whether the cabinet fans can maintain flow circulation inside the enclosed cabinet. The model is validated against a commercial code by using the same geometry and an air-cooled finned-coil heat exchanger object type. The exchanger duty and refrigerant outlet conditions agree to within 10%. Therefore, the model appears to be reasonably accurate for our system of interest.

The advantages of creating a custom, detailed model lies in its ability to capture the flow physics and problem domain with a high level of accuracy. For example, in this case, the pressure drop through the headers can be accurately computed by assigning the exact geometry. Moreover, such user-created models also allow the flexibility of tailoring the correlations used to better match the flow physics, an ability that commercial software such as Aspen EDR do not allow.

Finally, the validated model is used to study the effect of sub-cooling on the air-cooled evaporator performance. It is shown that an increase in sub-cooling leads to lower heat exchange between the hot air and cold refrigerant, which leads to higher air side exit temperatures for the same inlet temperature of 50 °C. This can be attributed to a greater degree of sensible versus latent cooling. An optimum value for the sub-cooling can be found for the target exit air temperature for a given set of inlet stream conditions of both fluids.

ACKNOWLEDGEMENTS

This material is based upon work supported by the NSF IUCRC Award No. IIP-1738782. Any opinions, findings, and conclusions or recommendations expressed in this material are those of the author(s) and do not necessarily reflect the views of the National Science Foundation.

The authors would like to thank Mr. Ken Allen of Super Radiator Coils and Mr. S.G. Schon of QuantaCool for permission to use Figures 2-3 and 4 upon modification, respectively.

REFERENCES

[1] Mohammad. Tradat, G. Mohsenian, Y. Manaserh, B. Sammakia, D. Mendo, and H. A. Alissa, “Experimental Analysis of Different Measurement Techniques of Server-Rack Airflow Predictions Towards Proper DC Airflow Management,” in *2020 19th IEEE Intersociety Conference on Thermal and Thermomechanical Phenomena in*

Electronic Systems (ITherm), Orlando, FL, USA, Jul. 2020, pp. 366–373. doi: 10.1109/ITherm45881.2020.9190584.

[2] M. I. Tradat, Y. "Mohammad A. Manaserh, B. G. Sammakia, C. H. Hoang, and H. A. Alissa, "An experimental and numerical investigation of novel solution for energy management enhancement in data centers using underfloor plenum porous obstructions," *Appl. Energy*, vol. 289, p. 116663, May 2021, doi: 10.1016/j.apenergy.2021.116663.

[3] ASHRAE, *THERMAL GUIDELINES FOR DATA PROCESSING ENVIRONMENTS*, 4th ed. ASHRAE, 2015.

[4] R. Miller, "Rack Density Keeps Rising at Enterprise Data Centers," *Data Center Frontier*, Apr. 27, 2020. https://datacenterfrontier.com/rack-density-keeps-rising-at-enterprise-data-centers/ (accessed Jun. 04, 2020).

[5] F. Limited, "Fujitsu Cool-Central Liquid Cooling Technology," presented at the ISC15, Frankfurt, Jul. 2015. [Online]. Available: https://www.fujitsu.com/global/Images/fujitsu-cool-central-liquid-cooling-technology.pdf

[6] D. Wu, J. B. Marcinichen, and J. R. Thome, "Experimental evaluation of a controlled hybrid two-phase multi-microchannel cooling and heat recovery system driven by liquid pump and vapor compressor," *Int. J. Refrig.*, vol. 36, no. 2, pp. 375–389, Mar. 2013, doi: 10.1016/j.ijrefrig.2012.11.011.

[7] J. B. Marcinichen, J. A. Olivier, and J. R. Thome, "On-chip two-phase cooling of datacenters: Cooling system and energy recovery evaluation," *Appl. Therm. Eng.*, vol. 41, pp. 36–51, Aug. 2012, doi: 10.1016/j.applthermaleng.2011.12.008.

[8] R. Khalid, S. G. Schon, A. Ortega, and A. P. Wemhoff, "Waste Heat Recovery Using Coupled 2-Phase Cooling Heat-Pump Driven Absorption Refrigeration," in *2019 18th IEEE Intersociety Conference on Thermal and Thermomechanical Phenomena in Electronic Systems (ITherm)*, May 2019, pp. 684–692. doi: 10.1109/ITHERM.2019.8757465.

[9] M. J. Moran and H. N. Shapiro, *Fundamentals of Engineering Thermodynamics*, 5th ed. Wiley & Sons, 2006.

[10] G. F. Davies, G. G. Maidment, and R. M. Tozer, "Using data centres for combined heating and cooling: An investigation for London," *Appl. Therm. Eng.*, vol. 94, pp. 296–304, Feb. 2016, doi: 10.1016/j.applthermaleng.2015.09.111.

[11] C. Mateu-Royo, J. Navarro-Esbrí, A. Mota-Babiloni, M. Amat-Albuixech, and F. Molés, "Theoretical evaluation of different high-temperature heat pump configurations for low-grade waste heat recovery," *Int. J. Refrig.*, vol. 90, pp. 229–237, Jun. 2018, doi: 10.1016/j.ijrefrig.2018.04.017.

[12] O. Bamigbetan, T. M. Eikevik, P. Nekså, M. Bantle, and C. Schlemminger, "Theoretical analysis of suitable fluids for high temperature heat pumps up to 125 °C heat delivery," *Int. J. Refrig.*, vol. 92, pp. 185–195, Aug. 2018, doi: 10.1016/j.ijrefrig.2018.05.017.

[13] J. L. Peureux, F. Sicard, and D. Bobelin, "French industrial heat pump developments applied to heat recovery," presented at the 11th IEA Heat Pump Conference, Montreal, Canada, May 2014.

[14] J. Rainer, D. Cibis, and H.-J. Laue, "Status And Outlook: Industrial Heat Pumps," presented at the International Refrigeration and Air Conditioning Conference, Purdue University, West Lafayette, IN, 2010. Accessed: Jun. 15, 2021. [Online]. Available: https://docs.lib.purdue.edu/iracc/1081/

[15] G. C. Bell, "Data Center Rack Cooling with Rear-door Heat Exchanger," Technology Case-Study Bulletin, Jun. 2010. [Online]. Available: https://datacenters.lbl.gov/sites/all/files/rdhx-doe-femp.pdf

[16] "Heat Exchangers | Coolcentric." http://www.coolcentric.com/heat-exchangers/ (accessed Jun. 05, 2020).

[17] "Rear Door Heat Exchangers," *Nortek Air Solutions*. /product/rear-door-heat-exchanger/ (accessed Jun. 05, 2020).

[18] "Liebert CRV, 19-40kW | Flexible In-Row Cooling." https://www.vertiv.com/en-ca/products-catalog/thermal-management/in-row-cooling/liebert-crv-in-row-cooling-system-19-40kw/#/models (accessed Jun. 05, 2020).

[19] F. C. McQuiston, "Finned Tube Heat Exchangers: State of the Art for the Air Side," presented at the 5th Annual Heat Pump Technology Conference, Oklahoma State University, Stillwater, Oklahoma, Apr. 1980.

[20] F. C. McQuiston, "Heat, Mass and Momentum Transfer Data For Five Plate-Fin-Tube Heat Transfer Surfaces," *ASHRAE Trans.*, vol. 84, no., pp. 266–293, 1978.

[21] D. G. Rich, "The Effect of Fin Spacing on the Heat Transfer and Friction Performance of Multi-Row, Smooth Plate-Fin-and-Tube Heat Exchangers," *ASHRAE Trans.*, vol. 79, no. 2, pp. 137–145, 1973.

[22] T. E. Schmidt, "La Production Calorifique des Surfaces Munies D'ailettes," *Bull. L'Institut Int. Froid*, vol. Annexe G-5, 1945.

[23] K. T. Hong and R. Webb, "Calculation of Fin Efficiency for Wet and Dry Fins," *HVACR Res.*, vol. 2, no. 1, pp. 27–41, Jan. 1996, doi: 10.1080/10789669.1996.10391331.

[24] S. G. Kandlikar, "An Improved Correlation for Predicting Two-Phase Flow Boiling Heat Transfer Coefficient in Horizontal and Vertical Tubes," presented at the 21st National Heat Transfer Conference, Seattle, WA, Jul. 1983.

[25] S. G. Kandlikar, "A General Correlation for Saturated Two-Phase Flow Boiling Heat Transfer Inside Horizontal and Vertical Tubes," *J. Heat Transf.*, vol. 112, no. 1, pp. 219–228, Feb. 1990, doi: 10.1115/1.2910348.

[26] M. M. Shah, "A general correlation for heat transfer during film condensation inside pipes," *Int. J. Heat Mass Transf.*, vol. 22, no. 4, pp. 547–556, 1979, doi: 10.1016/0017-9310(79)90058-9.

[27] W. M. Kays and A. L. London, *Compact Heat Exchangers*, 3rd ed. New York: McGraw- Hill, 1984.

[28] H. Qiao, "Transient modeling of a flash tank vapor injection heat pump system - Part I: Model development," *Int. J.*

Refrig., vol. 49, pp. 169–182, 2015, doi: 10.1016/j.ijrefrig.2014.06.019.
[29] T. H. Kuehn, J. W. Ramsey, and J. L. Threlked, *Thermal Environmental Engineering*, 3rd ed. Prentice Hall, 1998.
[30] F. C. McQuiston and J. P. Parker, *Heating Ventilating and Air-Conditioning-Analysis and Design*. New York: John Wiley & Sons, 1994.
[31] A. Zukauskus and R. Ulinskas, *"Banks of Plain and Finned Tubes", Heat Exchanger Design Handbook*, G.F. Hewitt Edition. New York: Begell House Inc., 1998.
[32] F. P. Incropera and F. P. Incropera, Eds., *Fundamentals of heat and mass transfer*, 6th ed. Hoboken, NJ: John Wiley, 2007.
[33] S. Levy, *Two-phase flow in complex systems*. New York: John Wiley, 1999.
[34] A. Husain, W. G. Choe, and J. Weisman, "The Applicability of the Homogenous Flow Model to Pressure Drop in Straight Pipe and Across Area Changes," Technical Report COO-2152-16, 1974.
[35] D. Butterworth, "A comparison of some void-fraction relationships for cocurrent gas-liquid flow," *Int. J. Multiph. Flow*, vol. 1, no. 6, pp. 845–850, 1975.
[36] S. L. Smith, "Void Fractions in Two-Phase Flow: A Correlation Based upon an Equal Velocity Head Model," *Proc. Inst. Mech. Eng. Part A*, vol. 184, no. 1, pp. 647–664, 1969, doi: 10.1243/PIME_PROC_1969_184_051_02.
[37] C. C. Hiller and L. R. Glicksman, "Improving Heat Pump Performance via Compressor Capacity Control-Analysis and Test," MIT, Technical Report 24525–96, 1976.
[38] H. Müller-Steinhagen and K. Heck, "A simple friction pressure drop correlation for two-phase flow in pipes," *Chem. Eng. Process. Process Intensif.*, vol. 20, no. 6, pp. 297–308, Nov. 1986, doi: 10.1016/0255-2701(86)80008-3.
[39] R. K. Shah and D. P. Sekulić, *Fundamentals of heat exchanger design*. Hoboken, NJ: John Wiley & Sons, 2003.
[40] "Aspen Exchanger Design and Rating EDR | AspenTech." https://www.aspentech.com/en/products/pages/aspen-exchanger-design-and-rating-edr (accessed Jun. 15, 2021).
[41] V. V. Wadekar, Y. S. Tian, and T. Kandlbinder, "Two-Phase Pressure Drop during Flow Boiling of Hydrocarbon Fluids," presented at the 5th European Thermal-Sciences Conference, Netherlands, 2008.
[42] "VARISTAR LHX 20_40.pdf." Accessed: May 10, 2021. [Online]. Available: https://csi.pl/wp-content/uploads/2019/01/VARISTAR%20LHX%2020_40.pdf
[43] I. H. Bell, J. Wronski, S. Quoilin, and V. Lemort, "Pure and Pseudo-pure Fluid Thermophysical Property Evaluation and the Open-Source Thermophysical Property Library CoolProp," *Ind. Eng. Chem. Res.*, vol. 53, no. 6, pp. 2498–2508, Feb. 2014, doi: 10.1021/ie4033999.
[44] "Welcome to CoolProp — CoolProp 6.4.1 documentation." http://www.coolprop.org/ (accessed May 10, 2021).